Lithos 204 (2014) 83–96

Contents lists available at ScienceDirect

Lithos

journal homepage: www.elsevier.com/locate/lithos

Late Paleozoic tectono–metamorphic evolution of the Altai segment of the Central Asian Orogenic Belt: Constraints from metamorphic P–T pseudosection and zircon U–Pb dating of ultra-high-temperature granulite

Zilong Li [a,*], Xiaoqiang Yang [a], Yinqi Li [a], M. Santosh [b], Hanlin Chen [a], Wenjiao Xiao [c]

[a] Department of Earth Sciences, Zhejiang University, Hangzhou 310027, PR China
[b] School of Earth Science and Resources, China University of Geoscience (Beijing), Beijing 100083, PR China
[c] Institute of Geology and Geophysics, Chinese Academy of Sciences, Beijing 100029, PR China

ARTICLE INFO

Article history:
Received 11 November 2013
Accepted 23 May 2014
Available online 2 June 2014

Keywords:
Ultra-high-temperature granulite
P–T pseudosection
Zircon U–Pb geochronology
Late Paleozoic
Altai orogenic belt

ABSTRACT

Ultra-high-temperature (UHT) granulite-facies rocks offer important constraints on crustal evolution processes and tectonic history of orogens. UHT granulites are generally rare in Phanerozoic orogens. In this study, we investigate the late Paleozoic pelitic UHT granulites from Altai in the western segment of the Central Asian Orogenic Belt (CAOB). The diagnostic minerals in these rocks include high alumina orthopyroxene (Al_2O_3 up to 9.76 wt.%, and y(opx) = Al^{VI} in orthopyroxene up to 0.21) coexisting with sillimanite and quartz, and low Zn spinel (ZnO = 1.85–2.50 wt.%) overgrowth with quartz. Cordierite corona separates sillimanite from orthopyroxene. The high alumina orthopyroxene is replaced by symplectites of low-alumina orthopyroxene (~5.80 wt.% Al_2O_3) and cordierite. These textural observations are consistent with a significant decompression following the peak UHT metamorphism. Phase equilibrium modeling using pseudosections and the y(opx) isopleths indicate an anti-clockwise P–T path for the exhumation of the Altai orogenic belt. The pre-peak assemblage of spinel + quartz in garnet is stable at high- to ultra-high-temperature and low-pressure conditions ($P < 5.8$ kbar at $T \sim 900$ °C). The peak P–T values recorded by high aluminium orthopyroxene is >940 °C and 7.8 to 10 kbar. Subsequent near-isothermal decompression occurred at 890 to 940 °C and 5 to 6 kbar. The final-stage cooling is recorded at 750 and 800 °C and 4 to 5 kbar accompanied by a decrease in the y(opx) values (0.11–0.12). In the UHT granulite, zircon grains are commonly enclosed within cordierite. The overgrowth rims of the zircon grains yield a weighted mean $^{206}Pb/^{238}U$ age of 277 ± 2 Ma using LA–ICP-MS zircon dating, which is interpreted to mark the timing of decompression and cooling. We propose that the anti-clockwise P–T path of the UHT granulite in the Altai orogenic belt could be related to an extensional event related to the sinistral strike-slip along the Irtish tectonic belt after the subduction and slab detachment during the convergence of the Kazakhstan–Junggar plate and the Siberian plate.

1. Introduction

Granulite-facies rocks that witnessed ultra-high-temperature (UHT) metamorphism at P–T conditions of >900 °C and 8–12 kbar are considered to represent crustal metamorphism at extreme thermal conditions (Harley, 2004, 2008; Kelsey, 2008; Santosh et al., 2012). The models for the formation of UHT granulites are diverse and equivocal, and include the following: back-arc spreading (Brown, 2006), post-collisional slab break-off and delamination (Santosh and Omori, 2008), orogenic self-heating (Clark et al., 2011; Nabelek et al., 2010), mantle plume, and ridge subduction (Santosh and Kusky, 2010). The diagnostic mineral assemblages of pelitic UHT granulites include sapphirine + quartz, orthopyroxene + sillimanite + quartz, low Zn spinel + quartz and osumilite, as reported from various UHT terranes (e.g., Dharma Rao et al., 2012; Shimizu et al., 2013; Tsunogae et al., 2011).

The mineral assemblages, textures, mineral compositions and geochronology recorded in UHT metamorphic rocks are widely used to decipher the P–T–t evolution and thermal history (Brown, 2007, 2014). However, owing to the extremely high temperature conditions and resetting of Fe–Mg during retrograde metamorphism, conventional geothermobarometric techniques to derive P–T conditions do not provide realistic estimates on the peak conditions of the UHT metamorphism. Instead, slow-diffusing cations such as Al, Ti, Si and Ca that are relatively immobile during retrograde re-equilibrium are more useful to derive precise P–T constraints (Pattison et al., 2003).

* Corresponding author at: Department of Earth Sciences, Zhejiang University, 38 Zheda Road, Hangzhou 310027, PR China. Fax: +86 571 87951580.
E-mail address: zilongli@zju.edu.cn (Z. Li).

http://dx.doi.org/10.1016/j.lithos.2014.05.022
0024-4937/

The 8000-km by 6000-km Central Asian Orogenic Belt (CAOB, Fig. 1) (also known as the Altaids, Central Asian Fold Belt or Central Asian Orogenic system) is one of the largest Phanerozoic accretionary orogens in the world, which formed by multiple accretion and amalgamation of allochthonous terranes (Windley et al., 2007; Xiao and Santosh, 2014; Xiao et al., 2010). The Altai orogenic belt in the westernmost part of the CAOB records a complex history of deformation, magmatism and metamorphism and is therefore an ideal target to investigate the tectonic history of the CAOB (Jiang et al., 2011; Tong et al., 2012; Wang et al., 2006; W. Wang et al., 2009; Wang et al., 2011; Wei et al., 2007; Xiao et al., 2010; Zheng et al., 2007). The metamorphic rocks in the Altai orogenic belt are associated with coeval magmatic suites and vary from greenschist- to granulite-facies, and rarely up to UHT granulite facies (Chen et al., 2006; Li et al., 2004, 2010a, 2010b; Wei et al., 2007; Zheng et al., 2007). The evolution of the Altai orogenic belt remains controversial, including the precise timing of termination of the Paleo-Asian ocean. The mechanism of the Permian thermal event is also debated such as extension in a post-orogenic setting (Tong et al., 2012; Wang et al., 2006; T. Wang et al., 2009), post island-arc environment (Xiao et al., 2009, 2010) and impact of the Tarim mantle plume (Zhang et al., 2012).

The UHT granulites in the Irtish tectonic belt (also known as Irtysh, Erqis, Irtishi, and Ertix) are a unique example of Phanerozoic UHT rocks in the CAOB, represent extremely high thermal conditions in the root of this orogen (Li et al., 2004, 2010a, 2010b). In this paper, we present metamorphic ages, pseudosection-based analyses of mineral stability and P–T conditions, and y(opx) (Al^{VI} in orthopyroxene) isopleths. The results enable us, for the first time, to construct the P–T–t path for the UHT crustal metamorphism (>940 °C), and discuss its significance in the tectonic evolution of the Altai orogenic belt during the late Paleozoic.

2. Geological background

The NW-SE trending Chinese Altai orogenic belt is bound by the Siberian plate to the north and the Kazakhstan–Junggar plate to the south (Windley et al., 2007; Xiao et al., 2010). Five fault-bound terranes have been identified based on the stratigraphy, metamorphism, deformation patterns and chronology (Fig. 1; He et al., 1990; Long et al., 2007; Windley et al., 2002; Yang et al., 2011). Terrane 1 mainly consists of the late Devonian to early Carboniferous meta-clastic rocks and limestone intercalated with minor arc-like volcanic rocks. Terrane 2 is composed of up-to-6000-m Neoproterozoic to the middle Ordovician sedimentary and volcanic rocks of the Habahe group (Yuan et al., 2007), and experienced lower greenschist-facies metamorphism. Terrane 3 in the central part of the Altai orogenic belt is the largest one and is mainly composed of early Silurian and early Devonian flysch sequence of the Habahe Formation (Long et al., 2010), among which, the ca. 502 Ma felsic volcanic rocks have been metamorphosed to greenschist- to upper amphibolite-facies (Windley et al., 2002; Yang et al., 2011). Terrane 4 consists of the late Silurian to early Devonian arc-like volcanic and pyroclastic rocks in the lower part and the middle Devonian turbidites and pillow-basalts in the upper part, showing a spectrum of metamorphic zones from greenschist to upper amphibolite. Terrane 5 is bordered by the Irtish fault to the south and is composed of a complex sequence of Precambrian basement, early Paleozoic to Devonian sediments and late Carboniferous volcanic clastic rocks, metamorphosed at greenschist- to amphibolite-facies conditions. Mafic

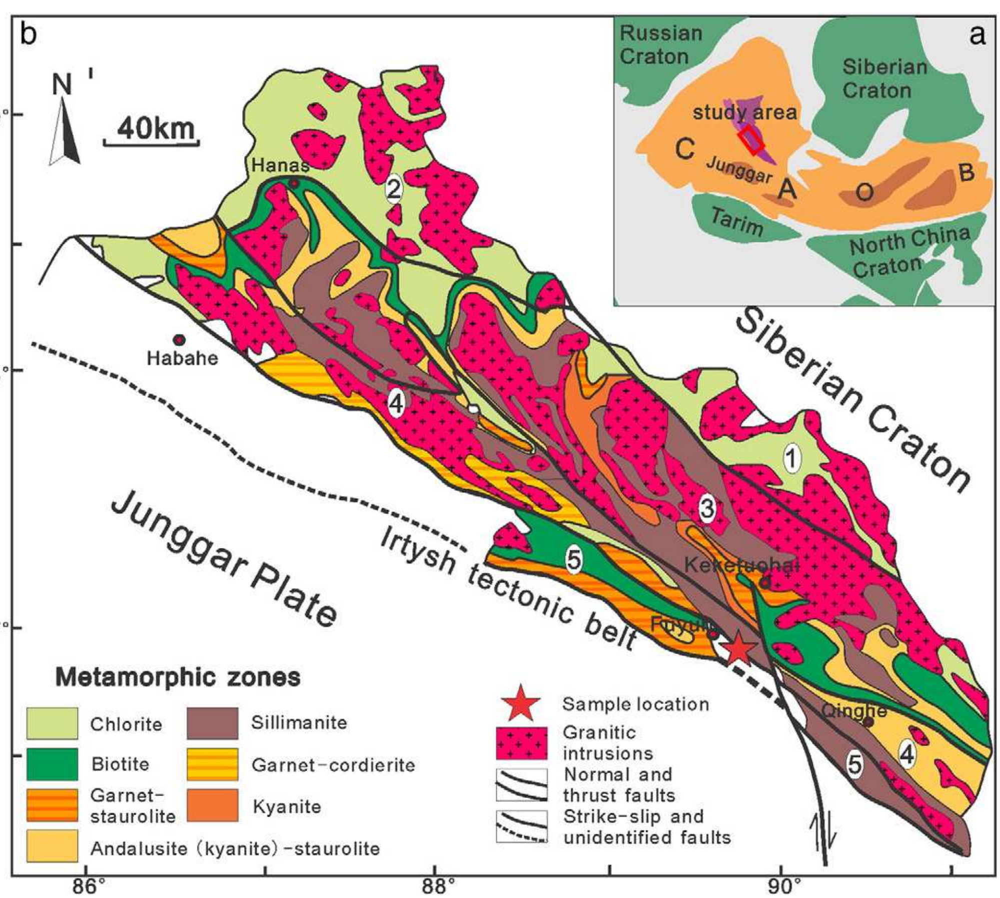

Fig. 1. Generalized geological framework of the central Asian Orogenic Belt (CAOB) (a) and the major metamorphic zones in the Altai orogenic belt (b). Modified after Wei et al. (2007).

granulite and UHT pelitic granulite were discovered in this terrane (Chen et al., 2006; Li et al., 2004, 2010a, 2010b). The Junggar plate to the south of the Irtish fault is composed of Devonian to Carboniferous volcanoclastics, which have been metamorphosed to greenschist-facies.

Two complex and progressive metamorphic zones of andalusite- and kyanite-types are documented in the Altai orogenic belt and are found to extend in all the terranes (Zhuang, 1994). The kyanite-type shows the sequence of biotite, garnet, staurolite, kyanite, sillimanite and locally garnet–cordierite zones. The andalusite-type includes biotite, garnet and staurolite zones at lower-temperature conditions, and sillimanite and garnet–cordierite zones at higher-temperature conditions, and also carries staurolite–andalusite and andalusite–sillimanite zones at intermediate-T conditions (Wei et al., 2007). The kyanite-type and andalusite-type metamorphic zones were considered to have developed in the burial and exhumation stages, respectively. Two metamorphic episodes during middle to early Devonian (~390 Ma, kyanite-type) and early to late Permian (andalusite-type) have been identified on the basis of recent geochronologic studies. A whole-rock Rb–Sr isochron age of 365 Ma has been reported from the high-grade schist and gneiss in Terrane 3 (Zhuang, 1994), which is interpreted as the metamorphic age (Windley et al., 2002). Zircon U–Pb ages of the high-grade gneiss in the eastern part of Terrane 4 are discordant and a lower intercept age of 367 ± 28 Ma is considered as the metamorphic age (Hu et al., 2002). Long et al. (2007) reported zircon $^{206}Pb/^{238}U$ ages between 388 Ma and 391 Ma of a garnet–sillimanite gneiss in Terrane 3 with a concordia age of 389 ± 2 Ma (MSWD = 1.2) and a mean age of 384 ± 6 Ma (MSWD = 4.3) from 11 spots of zircon grain overgrowth domains in a migmatite. SHRIMP zircon U–Pb ages of the sillimanite schist in the andalusite–sillimanite zone indicate that the andalusite-type metamorphism occurred at 299.2 ± 3.4 Ma (Wang et al., 2013). The low-pressure pelitic granulite with mineral association of spinel + cordierite in the sillimanite zone of the Altai orogenic belt was dated as 292.8 ± 2.8 Ma (W. Wang et al., 2009).

The broad tectonic framework of the Altai region involves three main stages (Chen and Jahn, 2002; He et al., 1990; Windley et al., 2007; Yang et al., 2011); (i) a peri-Gondwana terrane during Neoproterozoic to Early Paleozoic; (ii) Early Ordovician to late Devonian (375 Ma), arc magmatism on a continental arc margin; and (iii) Permian (290–270 Ma) post-orogenic setting coupled with the sinistral strike-slip of the Irtish belt, with a possible overprinting by the Tarim mantle plume (Zhang et al., 2012).

The UHT granulite in Terrane 5 of the Altai orogenic belt occurs as an elongated lens of ca. 0.5 m width, and is enclosed in a garnet–biotite gneiss striking N 206–210° with steep dips of 67–70° (Fig. 2). The country rocks, composed of a biotite–plagioclase gneiss and a garnet–biotite gneiss, were intruded by fine-grained granitic dikes. All the rock types were subjected to intense deformation and their foliations show similar orientation.

3. Petrography

The Altai UHT granulite shows porphyroblastic texture and gneissic structure and is mainly composed of garnet (15–20%), orthopyroxene (8–15%), cordierite (10–20%), biotite (15–20%), plagioclase (10–20%), quartz (10–25), ilmenite (3–5%), sillimanite (5–7%), spinel (<2%) and zircon. The foliation is defined by the orientation of sillimanite and biotite. Some garnet grains are stretched parallel or sub-parallel to the main foliation. The aluminous domains are composed of garnet + orthopyroxene + sillimanite + cordierite + biotite + plagioclase + quartz ± spinel ± ilmenite, which alternate with felsic layers of biotite + plagioclase + quartz ± sillimanite.

Garnet diablastic grains have sizes ranging from 1 to 7 mm and contain subhedral to anhedral mineral inclusions of sillimanite, spinel, ilmenite and quartz (Fig. 3c). Euhedral to subhedral coarse-grained (0.1–0.5 mm) orthopyroxene porphyroblasts are well preserved. Two stages of orthopyroxene are recognized based on their occurrence and textural association; the first stage is a brownish yellow to light yellow pleochroic variety (Opx1), and the second stage is a light yellow variety (Opx2) that commonly coexists with cordierite. Opx1 is often surrounded by Opx2 (Fig. 3e, f and g). Biotite shows light to dark brown pleochroism, typical of high-temperature metamorphic origin, and it occurs as a breakdown phase surrounding orthopyroxene or along cracks in garnet (Fig. 3a and b). Cordierite commonly occurs as corona that mantles the peak mineral assemblage of garnet (Fig. 3c), orthopyroxene (Fig. 3d) and sillimanite (Fig. 3f). Cordierite typically contains mineral inclusions of biotite, sillimanite, spinel and zircon (Fig. 3c, e and f). Granular spinel is intergrowth with ilmenite grains and occurs in two associations, one is small granular spinel seen as

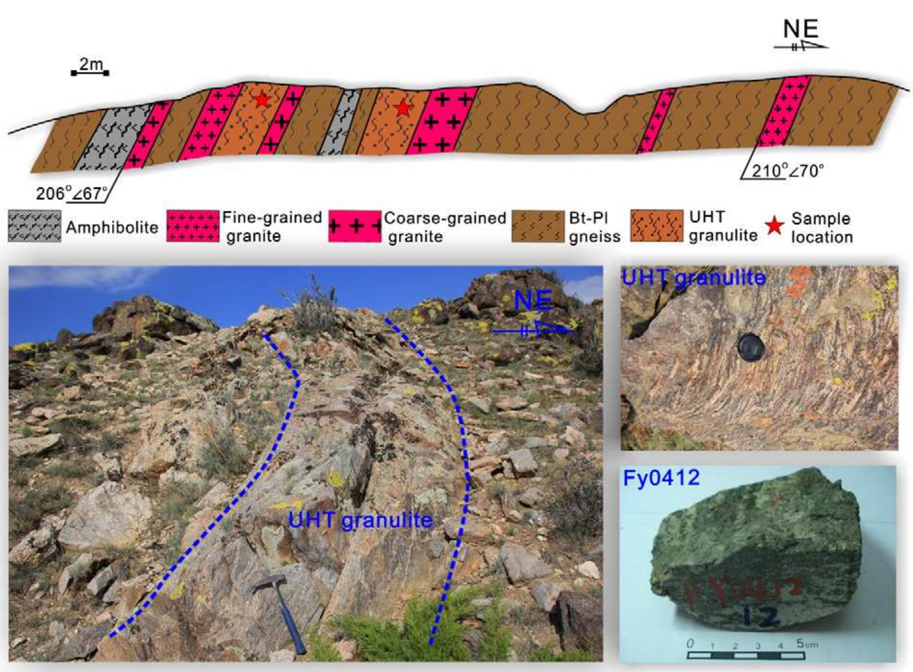

Fig. 2. A cross section showing the occurrence of the UHT granulite in the Altai orogenic belt.

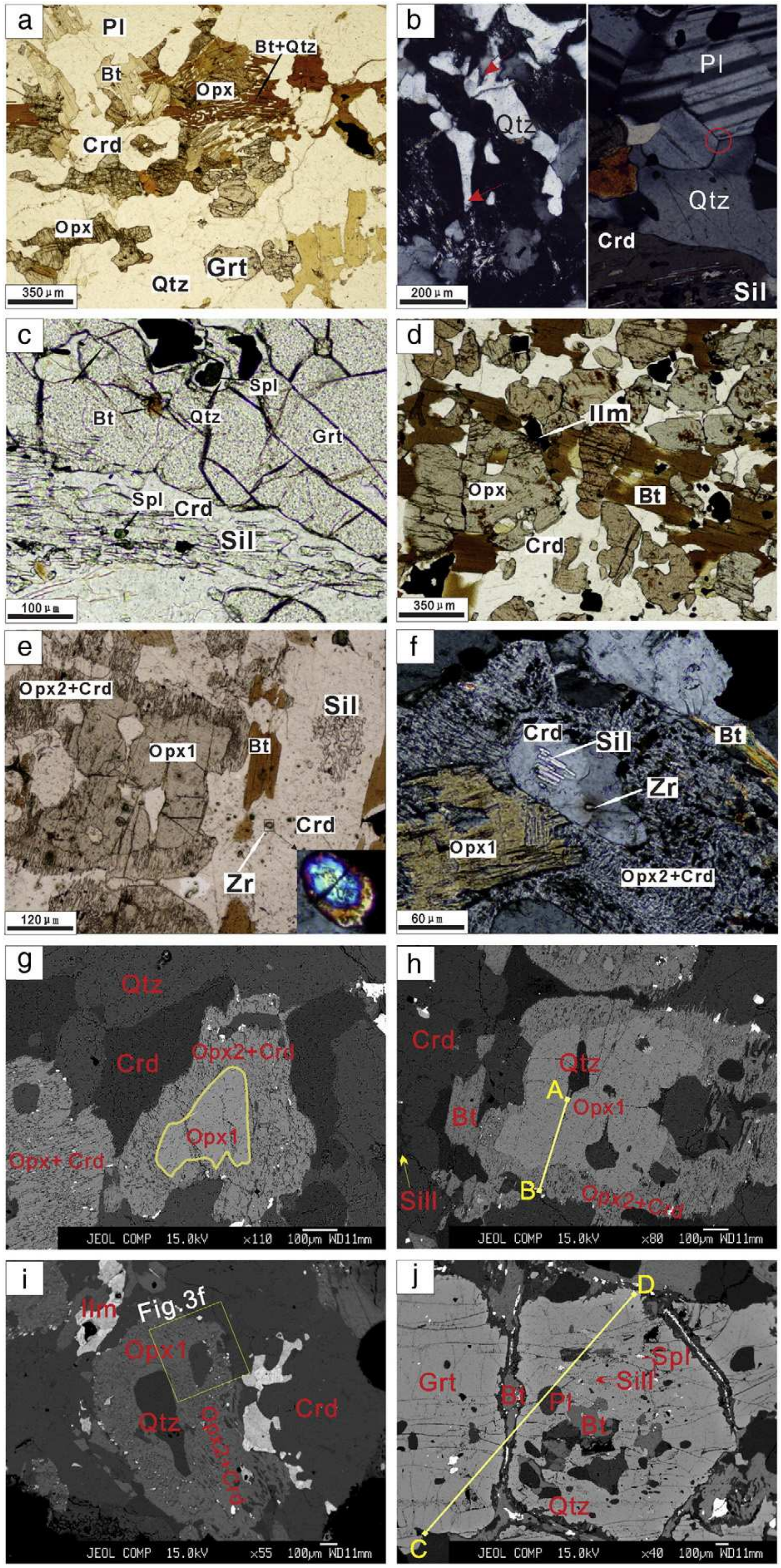
a
Pl
Bt+Qtz
Bt
Opx
Crd
Opx
Qtz
Grt
350 μm
b
Qtz
Pl
Qtz
Crd
Sil
200 μm
c
Spl
Bt
Qtz
Grt
Spl
Crd
Sil
100 μm
d
Ilm
Opx
Bt
Crd
350 μm
e
Opx2+Crd
Sil
Opx1
Bt
Crd
Zr
120 μm
f
Crd
Sil
Bt
Zr
Opx1
Opx2+Crd
60 μm
g
Qtz
Crd
Opx2+Crd
Opx1
Opx+ Crd
JEOL COMP 15.0kV ×110 100μm WD11mm
h
Crd
Qtz
A
Opx1
Bt
Sill
B
Opx2+Crd
JEOL COMP 15.0kV ×80 100μm WD11mm
i
Ilm
Fig.3f
Opx1
Qtz
Opx2+Crd
Crd
JEOL COMP 15.0kV ×55 100μm WD11mm
j
D
Spl
Sill
Grt
Bt
Pl
Bt
Qtz
C
JEOL COMP 15.0kV ×40 100μm WD11mm

inclusions along with biotite or quartz in the core of garnet (Fig. 3c), and the other is as inclusions in cordierite in the matrix. Plagioclase and quartz in the felsic layers show low dihedral angles against surrounding minerals (Fig. 3b, left) or eutectic textual equilibrium (Fig. 3b, right) in local domains, indicating melt crystallization at a different pressure/depth (Holness et al., 2011).

The granulite has diagnostic UHT assemblages of orthopyroxene (Opx1) + sillimanite + quartz and spinel + quartz, which are inferred to have formed at peak condition (M1). The sillimanite is the only phase of aluminosilicate, and therefore the peak metamorphism is considered to have occurred in the stability field of sillimanite. The assemblage of orthopyroxene (Opx2) + cordierite ± biotite and sillimanite + spinel + cordierite ± biotite formed at the retrograde stage (M2), as inferred from the zoned Opx1 separated from sillimanite by cordierite (Fig. 3f), and replaced by symplectite of orthopyroxene (Opx2) + cordierite (Fig. 3g, h and i). The edges of garnet grains are commonly replaced by sillimanite + spinel + cordierite (Fig. 3c), consistent with a retrograde reaction. Garnet contains inclusions of sillimanite, ilmenite and spinel. The coexistence of spinel + quartz in the core of garnet (Fig. 3c) may represent the pre-peak condition (M0).

4. Analytical methods

Five representative samples (Fy0401, Fy0402, Fy0406, Fy0411 and Fy0412) with diagnostic UHT assemblages were selected for this study. Zircon grains were separated from four samples (Fy0402, Fy0412, Fy052116 and Fy052117) for LA–ICP-MS U–Pb dating.

4.1. Mineral composition

Mineral compositions were analyzed on polished thin sections using a JEOL JXA-8100 electron probe microanalyzer (EPMA) at the Key Laboratory of the Second Institute of Oceanography of the State Oceanic Administration in Hangzhou, China. Quantitative analysis was carried out following the procedure and analytical conditions adopted by Iizuka and Hirata (2005). The operating conditions are 15 kV acceleration voltage and 10 nA beam current. The beam diameter was set to 2 μm for all minerals and the peak counting of upper and lower baselines for all elements was set for 20 s and 10 s, respectively.

4.2. LA–MC-ICP-MS zircon U–Pb dating

Zircon grains were extracted by crushing and concentration following standard density and magnetic separation procedures. Handpicked zircon grains together with TEMORA standard (417 Ma, for quality control) were mounted in an epoxy mount and then polished down to expose grains. The cathodoluminescence (CL) and backscattered electron (BSE) images were obtained using a Hitachi S3000N scanning electron microscope (SEM) at the Institute of Geology, Chinese Academy of Geosciences, in order to identify internal textures and choose potential target sites for U–Pb analyses.

Zircon U–Pb isotopic dating was performed on a laser ablation multi-collector inductively coupled plasma mass spectrometer system (LA–MC-ICP-MS) at the Isotope Laboratory of Tianjin Institute of Geology and Mineral Resources, using a Thermo Fisher Neptune MC-ICP-MS coupled with a UP193-FX ArF exciter laser (ESI, US). Spot size is 35 μm in this study. Helium was used as the carrier gas to enhance the transport efficiency of ablated material. Data were acquired for 20 s with the laser off and 40 s with the laser on. Raw rate was calibrated by an internal standard and NIST 612 as the reference standard. Ratios were corrected for both instrumental mass bias and elemental and isotopic fractionation by using an external standard. Ages and concordia diagrams were prepared using ISOPLOT 4.1 (Ludwig, 2009).

5. Zircon morphology and U–Pb ages

Zircon grains from the Altai UHT granulites are colorless and transparent under a microscope. Based on the backscattered electron (BSE) and CL images (Fig. 4), two types of zircon grains are recognized. Type 1 zircon grains are rounded or irregular in shape and exhibit a light and homogeneous luminescence around a dark resorbed core with or without oscillatory zoning. The light rims are interpreted to be the metamorphic overgrowth (e.g., spots 1, 2 and 3 in sample Fy0402). Type 2 zircons are subhedral to euhedral prismatic grains with concentric zoning in local domains, consistent with an igneous origin (e.g., spots 29 and 31 in sample Fy0412). Type 1 zircon grains occur in all the four samples, whereas Type 2 grains are more common in samples Fy0412 and Fy052116.

A total of 147 spots were analyzed on 112 grains from the four samples (Supplementary Table 1), and most spots were analyzed for the rim of Type 1 zircon grains. The majority of spot ages are concordant or nearly concordant regardless of the pre-Neoproterozoic grains (Fig. 5). The ages of the rims for Type 1 zircon grains from sample Fy0402, Fy0412 and Fy052117 cluster at ~280 Ma, and define a weighted mean $^{206}Pb/^{238}U$ age of 277 ± 2 Ma with 95% confidence (43 spots, Fig. 6). The rim ages for the zircon grains from sample Fy052116 are clustered at 390 Ma.

6. Mineral compositions

6.1. Orthopyroxene

Orthopyroxene grains with a different size and texture have variable Al_2O_3 contents (Table 1). The core of the orthopyroxene porphyroblast (Opx1) shows >8.0 wt.% Al_2O_3 with a maximum of 9.76 wt.% and X_{Mg} in the range of 0.65–0.68, whereas the porphyroblastic rim and symplectitic orthopyroxene (Opx2) have lower Al_2O_3 (<8.0 wt.%) and lower X_{Mg} values (generally <0.65). Aluminium in orthopyroxene is expressed as y(opx), which is calculated as $Cation_{Al,total(opx)}$ / 2. The y(opx) values vary from 0.21 to 0.07 with a decrease of X_{Mg} from 0.66 to 0.63 (Fig. 7).

6.2. Garnet

Garnet is an almandine-pyrope solid solution (Table 2) with typical granulite-facies diffusion zoning (Spear, 1993). The X_{Mg} values (Mg / (Mg + Fe), mole ratio) in coarse-grained garnet are nearly constant (~0.48) in the core and show an abrupt shift when adjacent to biotite and cordierite or towards the rim, indicating re-equilibration during retrograde metamorphism in local domains. For example, X_{Mg} values in the core and rim part of the garnet in sample Fy0401 (Fig. 8) range from 0.43 to 0.48 and 0.27 to 0.44, respectively, whereas the spessartine and grossular end-member components are <5%.

6.3. Other minerals

Cordierite has X_{Mg} values ranging from 0.75 to 0.84 (Table 3). A systematic X_{Mg} trend is not observed in the cordierite coronas. Biotite

Fig. 3. Photomicrographs (a–f) and backscattered electron images (g–j) of the Altai UHT granulite. (a) An assemblage of garnet and orthopyroxene with local replacement of cordierite and biotite, sample Fy052116, PPL; (b) possible granitic melt in the felsic domain as noted with the red arrow (left, Fy0412) and circle (right, Fy052117), CPL; (c) garnet porphyroblast containing inclusions of ilmenite, spinel, quartz and biotite, while spinel and sillimanite occur as inclusions in cordierite (Fy052117), PPL; (d) orthopyroxene is replaced by biotite (Fy052117), CPL; (e and f) orthopyroxene and sillimanite separated by cordierite corona. Zircons are enclosed in the corona. High alumina orthopyroxene (opx1) is replaced by symplectite of low-alumina orthopyroxene (opx2) and cordierite (Fy0401), PPL and CPL; (g, h and i) different occurrences of high alumina orthopyroxene replaced by symplectite of cordierite and low alumina orthopyroxene and surrounded by the cordierite corona (Fy0401); (j) garnet porphyroblast containing inclusions of spinel, quartz, plagioclase, biotite and quartz (Fy0401). PPL: plane-polarized light, CPL: cross-polarized light.

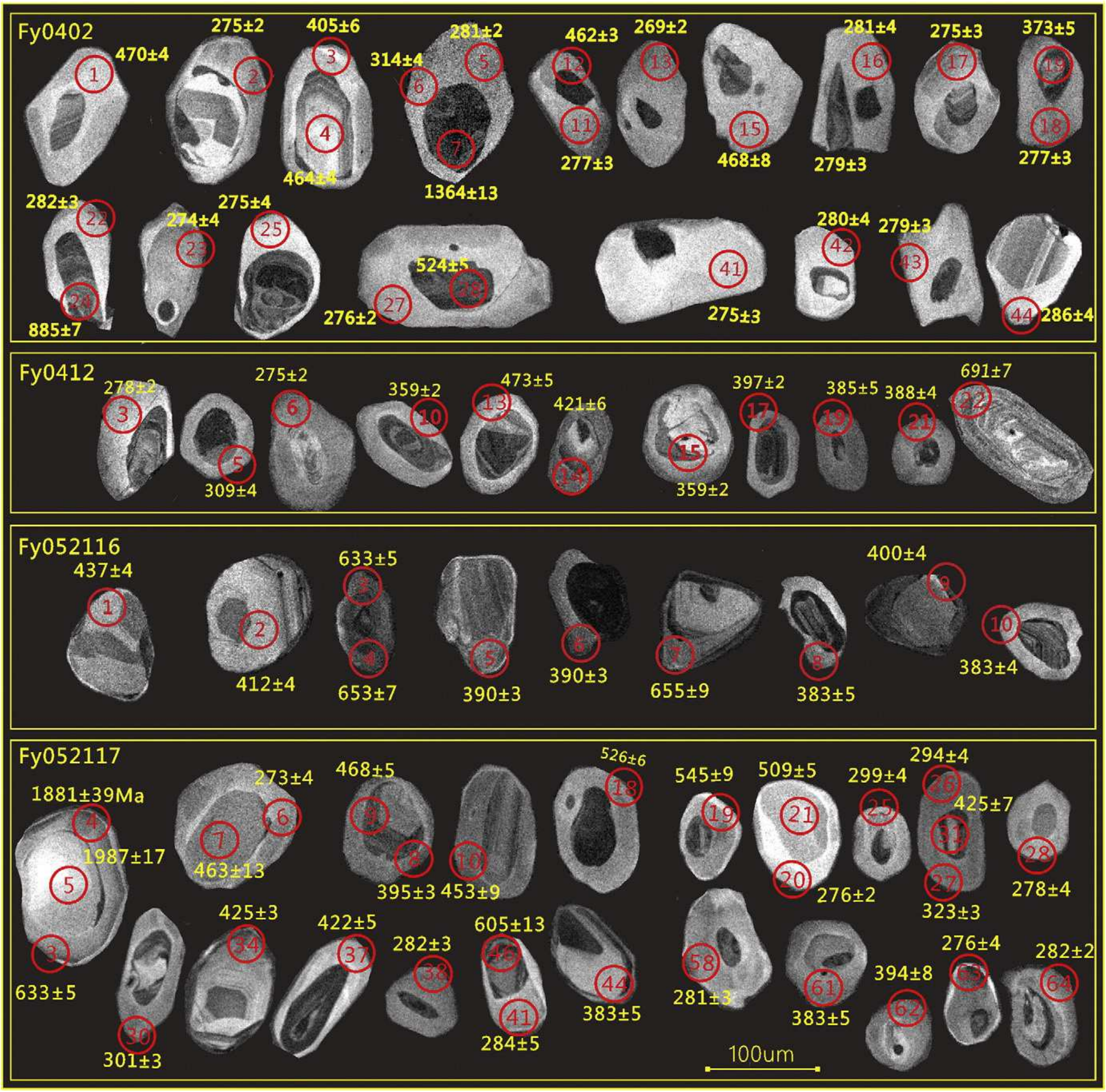

Fig. 4. Cathodoluminescence images and $^{206}Pb/^{238}U$ ages of the zircon grains.

is rich in Mg with X_{Mg} varying from 0.53 to 0.70. The biotite grains have 2.33–4.88% TiO_2. The biotite grains that are directly in contact with garnet have higher X_{Mg} (>0.7) than those in the matrix (X_{Mg} = 0.6–0.7). Spinel grains have low X_{Mg} values (0.26–0.32) compared with other ferromagnesian minerals. The spinel grains have 1.1–2.8 wt.% ZnO. The spinel grains that coexist with quartz have ZnO higher than those in contact with ilmenite (Li et al., 2010b). Plagioclase is Na-rich, with anorthite/albite ratios ranging from 27/72 to 35/64.

7. P–T pseudosection

The P–T conditions and metamorphic evolution of the Altai UHT granulite are investigated using pseudosection, based on THERMOCALC version 3.33 (Powell and Holland, 1988) and internally consistent thermodynamic dataset ds55 (Holland and Powell, 1998; updated in November 2003). The calculation was based on the system Na_2O–CaO–K_2O–FeO–MgO–Al_2O_3–SiO_2–H_2O–TiO_2–Fe_2O_3 (NCKFMASHTO), which is broadly consistent with the natural system so that melt-bearing equilibrium can be calculated. A decrease in elemental efficiency during the process of melt loss and cooling may result in the development of chemical–mineralogical microdomains. The effective bulk composition was obtained by using the elemental mapping of an appropriate domain in a thin section under the electron microprobe as suggested by Clarke et al. (2001). The effective bulk composition used in the P–T pseudosection in this study was derived from the microdomain composed of coexisting orthopyroxene, sillimanite, cordierite and biotite with an excess of plagioclase and quartz, based on their relative area (Fig. 9a). This approach may overestimate the porphyroblast and underestimate the matrix but would not affect the main topology of the mineral assemblage, especially the low variance assemblages (Alvarez-Valero and Waters, 2010). The a–x models in this study is based on the cordierite data from Holland and Powell (1998), ilmenite

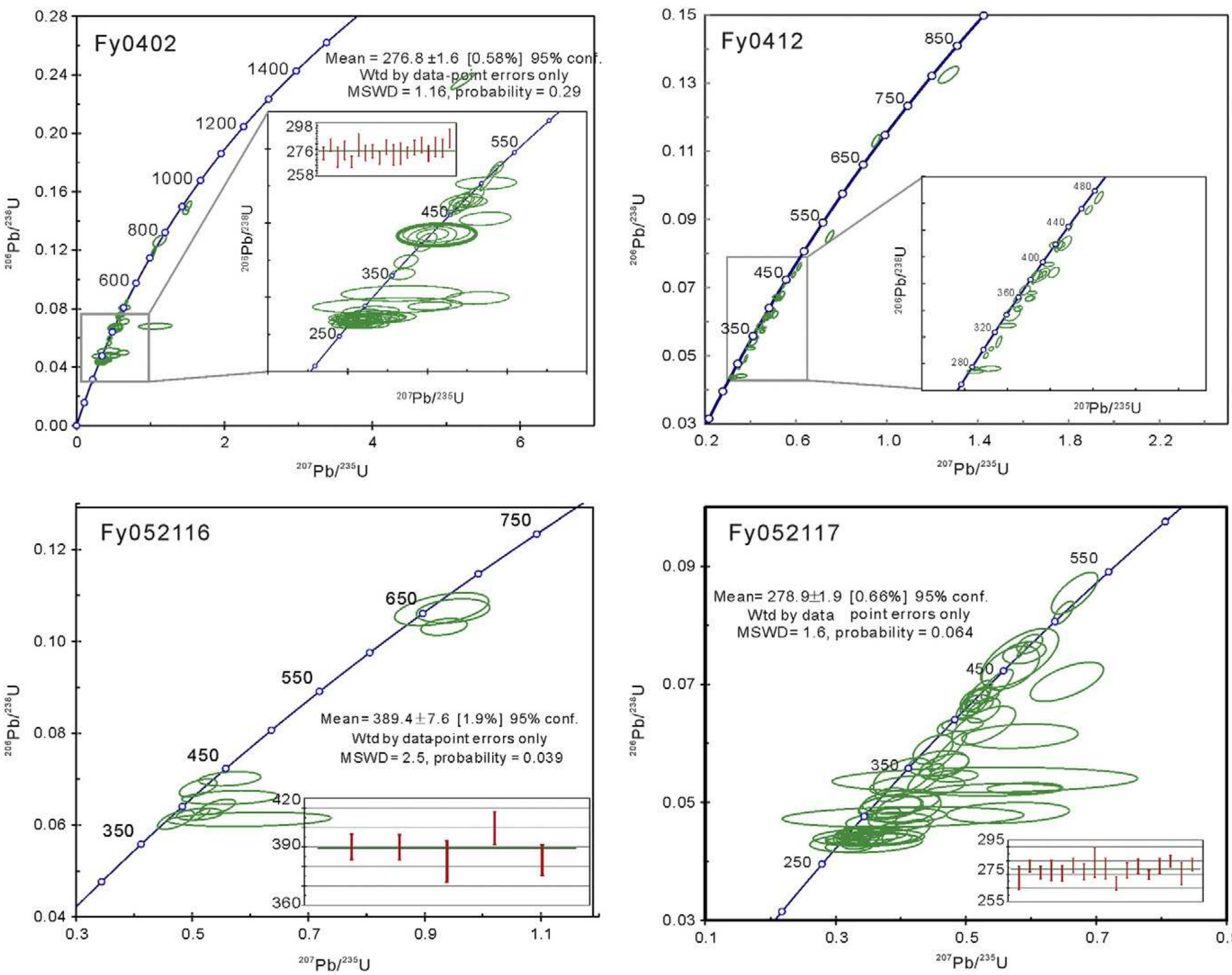

Fig. 5. Concordia of zircon U–Pb ages.

from White et al. (2000), orthopyroxene from White et al. (2002), plagioclase and K-feldspar from Holland and Powell (2003), and garnet, silicate melt and biotite from White et al. (2007). Quartz, sillimanite and kyanite are considered as pure phases. The effect of water and the retrograde metamorphic history was evaluated by using two T–M_{H2O} pseudosections with the same composition as for the P–T pseudosection under 8.5 kbar and 5 kbar, respectively (Fig. 9b and c). Introduction of Ti (NCKFMASHTO) would mainly affect the temperature range of biotite (up to 900 °C), which is not stable under the peak condition. Hence, a P–X_{Mg} pseudosection diagram (Fig. 9d) was constructed in a simplified

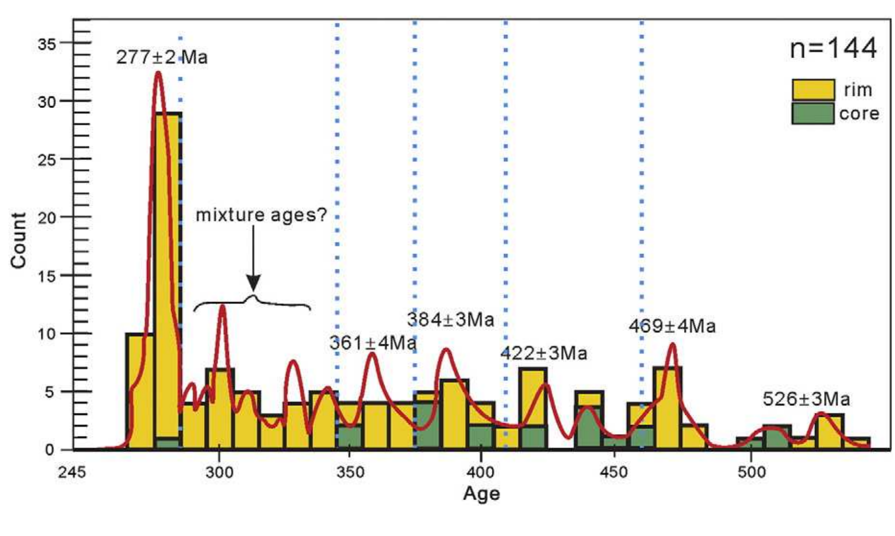

Fig. 6. Histograms and relative probability of zircon U–Pb ages.

Table 1
Representative compositions of orthopyroxenes from the Altay UHT granulite.

Sample no.	Fy0401	Fy0401	Fy0406	Fy0406	FY0406	Fy0407	Fy0407	Fy0412	Fy0412
Analysis	26-core	518-rim	524-rim	530-rim	441-rim	337-core	338-rim	44-core	41-core
SiO_2	48.41	50.55	49.33	51.00	52.11	49.71	51.47	48.47	48.65
TiO_2	0.11	0.04	0.05	0.09	0.13	0.05	0.09	0.15	0.10
Al_2O_3	9.08	4.84	6.24	4.35	6.73	7.39	5.24	9.76	8.81
FeO^T	23.20	24.65	26.12	24.46	20.49	22.90	23.19	21.61	21.85
MnO	0.18	0.24	0.18	0.22	0.24	0.08	0.20	0.09	48.65
MgO	20.24	20.37	18.97	21.59	19.44	21.06	21.43	20.41	20.77
CaO	0.08	0.10	0.08	0.15	0.28	0.05	0.06	0.05	0.02
Na_2O	0.02	0.01	0.00	0.02	0.62	0.03	0.01	0.00	0.06
K_2O	0.00	0.00	0.01	0.02	0.00	0.01	0.01	0.00	0.00
Cr_2O_3	0.00	0.00	0.00	0.00	0.00	0.03	0.00	0.00	0.00
Total wt.%	101.32	100.80	100.96	101.89	100.05	101.30	101.72	100.54	100.35
No. oxygen	6	6	6	6	6	6	6	6	6
Si	1.78	1.88	1.85	1.88	1.91	1.83	1.88	1.78	1.79
Al	0.39	0.21	0.28	0.19	0.29	0.32	0.23	0.42	0.39
Ti	0.00	0.00	0.00	0.00	0.00	0.00	0.00	0.00	0.00
Fe^{3+}	0.03	0.02	0.02	0.05	0.00	0.03	0.00	0.00	0.03
Fe^{2+}	0.68	0.75	0.79	0.70	0.63	0.68	0.71	0.66	0.65
Mn	0.01	0.01	0.01	0.01	0.01	0.00	0.01	0.00	0.00
Mg	1.11	1.13	1.06	1.19	1.06	1.15	1.17	1.12	1.15
Ca	0.00	0.00	0.00	0.01	0.01	0.00	0.00	0.00	0.00
Na	0.00	0.00	0.00	0.00	0.04	0.00	0.00	0.00	0.00
K	0.00	0.00	0.00	0.00	0.00	0.00	0.00	0.00	0.00
Total	4.02	4.01	4.01	4.03	3.96	4.01	4.00	4.00	4.02
X(Mg)	0.62	0.60	0.57	0.63	0.63	0.63	0.62	0.63	0.64
y(opx)1	0.20	0.11	0.14	0.09	0.15	0.16	0.11	0.21	0.19
y(opx)2	0.18	0.10	0.12	0.07	0.20	0.15	0.11	0.21	0.18
$Fe^{3+}/(Fe^{3+}+Fe^{2+})$	0.05	0.02	0.03	0.07	0.00	0.04	0.00	0.00	0.05

system of NCKFMASH to evaluate the effect of heterogeneous bulk compositions on the formation of different mineral assemblages in the Altai UHT granulite with composition (except for FeO and MgO) derived from whole rock analysis.

A representative P–T pseudosection based on a representative orthopyroxene–sillimanite microdomain at 700 to 1050 °C and 2 to 12 kbar is shown in Fig. 9a. Quartz, plagioclase and ilmenite are stable and appear in all fields except for the high-T fields. Garnet is stable at >5.5 kbar and 750 °C, and the garnet-in line gradually increases to 7 kbar at UHT conditions. Orthopyroxene is stable in low to intermediate pressure (2–10 kbar) with orthopyroxene-out line around 10 kbar at >900 °C. Cordierite appears in lower pressure (generally <7 kbar), with cordierite-in line starting from 5.8 kbar at 700 °C and reaching 8.2 kbar at 890 °C, and then dropping to 7.3 kbar at 980 °C. The mole proportion of K-feldspar shown in the P–T pseudosection is <0.05.

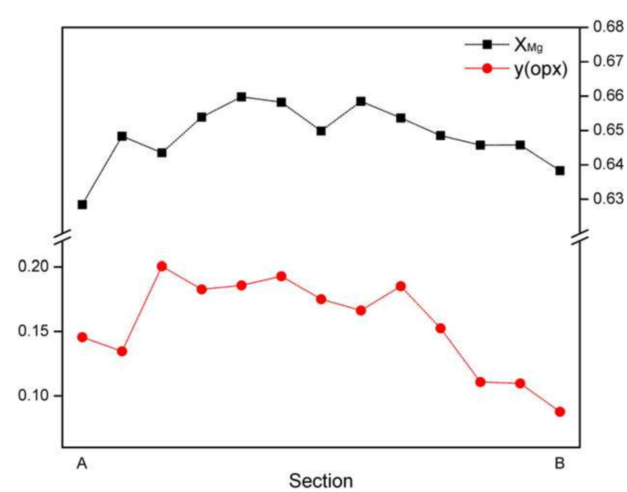

Fig. 7. (a) Profiles of X_{Mg} and y(opx) zoning patterns in the section A–B from porphyroblastic orthopyroxene in sample Fy0401.

This is partly because the pseudosection was modeled under a relatively dry and closed system. Meanwhile, T–M_{H2O} pseudosections under 8.5 kbar and 5 kbar (Fig. 9b and c) reveal that the y(opx) isopleths (>0.12) are perpendicular or near perpendicular to the temperature axis, i.e., the y(opx) isopleths are dependent on the mineral assemblages. Therefore, the water content and the appearance of K-feldspar in the pseudosection would not significantly affect the estimation of P–T conditions.

The peak mineral assemblage (M1) of high-Al orthopyroxene + sillimanite + garnet + plagioclase + quartz + ilmenite (±quartz) are in equilibrium at >7 kbar and >910 °C, consistent with the equilibrium condition of 8 to 9 kbar and >900 °C (Kelsey, 2008). The y(opx)values are up to 0.21 (Supplementary Table 1), which yield a temperature >940 °C. Therefore, the peak stage (M1) is defined at T > 940 °C and 7.8 to 10 kbar, consistent with the decrease of y(opx) values (0.21 to 0.19). The X_{Mg} of orthopyroxene in the peak stage calculated from THERMOCALC is >0.70, although this is not preserved probably due to later Fe–Mg exchange with other minerals.

The post-peak stage (M2a) was recorded by the breakdown of garnet and the formation of cordierite corona. This is illustrated by the P–T path that cuts across the garnet-out line and cordierite-in line in pseudosection. The compositional zoning of X_{Mg} and y(opx) in the orthopyroxene decreases to 0.66 to 0.67 and 0.15 to 0.19 respectively, associated with a significant decrease of pressure to 5–6 kbar and a slight decrease of temperature to 890–940 °C.

The final stage (M2b) of retrograde metamorphism mainly involved the formation of biotite under solidus condition. Low-Al orthopyroxene with a y(opx) value of 0.09 to 0.11 and the composition of plagioclase yielded the retrograde conditions (M2b) of 750 to 800 °C and 4 to 5 kbar. This stage is probably associated with the addition of H_2O (Fig. 9c), a common process during the retrograde stage (Guiraud et al., 2001). This may explain the rare occurrence of K-feldspar in the Altai UHT granulite.

A P–X_{Mg} pseudosection based on the bulk composition was constructed at 900 °C and 4 to 10 kbar with the X_{Mg} value increasing from 0 to 0.8 (Fig. 9d). At the same mole ratio of $Al_2O_3/(Al_2O_3 + FeO + MgO)$, the

Table 2
Representative compositions of garnet and cordierite from the Altay UHT granulite.

Sample no.	FY0401	FY0401	FY0412	FY0406	FY0406	FY0406	FY0412	FY0412
Analysis	383	460	265	516*-rim	541-core	528-rim	543-core	548*-rim
Mineral	Cordierite	Cordierite	Cordierite	Garnet	Garnet	Garnet	Garnet	Garnet
SiO_2	49.96	50.39	49.84	37.89	39.76	38.73	39.92	39.12
TiO_2	0.02	–	0.02	0.08	0.12	0.05	0.10	0.08
Al_2O_3	33.59	33.53	33.40	21.37	22.77	22.07	22.38	22.32
FeO^T	4.17	4.10	3.79	31.60	23.69	28.10	24.17	26.03
MnO	0.06	–	0.02	0.98	0.52	0.64	0.58	0.56
MgO	11.57	11.41	11.45	6.46	12.16	8.99	12.34	11.15
CaO	0.02	0.05	0.03	1.09	0.85	1.12	0.83	0.84
Na_2O	0.13	0.11	0.08	–	–	–	0.02	–
K_2O	0.01	0.02	–	0.01	0.01	–	–	–
Cr_2O_3	–	–	0.05	–	–	–	–	–
Total wt.%	99.53	99.60	98.67	99.48	99.88	99.70	100.33	100.09
No. oxygen	18	18	18	12	12	12	12	12
Si	4.99	5.02	5.01	3.00	3.00	2.99	3.00	2.98
Al	3.95	3.94	3.95	1.99	2.02	2.01	1.98	2.00
Ti	–	–	–	–	0.01	–	0.01	–
Fe^{3+}	–	–	–	0.01	–	–	–	0.03
Fe^{2+}	0.35	0.34	0.32	2.08	1.49	1.82	1.52	1.63
Mn	0.01	–	–	0.07	0.03	0.04	0.04	0.04
Mg	1.72	1.69	1.71	0.76	1.37	1.04	1.38	1.27
Ca	0.00	0.01	0.00	0.09	0.07	0.09	0.07	0.07
Na	0.03	0.02	0.02	–	–	–	–	–
K	–	–	–	–	–	–	–	–
Cr	–	–	–	–	–	–	–	–
Total	11.05	11.02	11.02	8.00	7.99	8.00	8.00	8.02
X(Mg)	0.83	0.83	0.84	0.27	0.48	0.36	0.48	0.44
Alm	–	–	–	69.39	50.42	60.83	50.54	54.31
Spess	–	–	–	2.19	1.12	1.40	1.23	1.20
Pyro	–	–	–	25.36	46.16	34.67	46.01	42.20
Gross	–	–	–	3.06	2.31	3.09	2.21	2.29

spinel and quartz assemblage in garnet is stable under the low-X_{Mg} side (<0.28), whereas the paragenesis of orthopyroxene, sillimanite and garnet appears in the high X_{Mg} side (>0.62).

The association of low-Zn spinel + quartz is considered as one of the UHT indicators in the Altai orogenic belt (Li et al., 2010b), and the assemblage is stable under high- to ultra-high-temperature and lower pressure in the KFMASHZn system (Kelsey, 2008; Nichols et al., 1992). As shown in the P–X_{Mg} pseudosection, the spinel + quartz association is stable under <5.7 kbar and 900 °C for the given bulk composition (Fig. 9d). Combined with the inclusions of low-Zn spinel + quartz in garnet and the replacement of garnet with spinel + sillimanite + cordierite (Fig. 3c and f), these textures may have been formed by the compression and decompression processes at a relative high temperature (~900 °C) during the prograde and retrograde metamorphic stages, respectively. The compositions of the garnet in the garnet + sillimanite assemblage developed in a low-X_{Mg} microdomain have a difficulty constraining the peak stage owing to the strong Fe–Mg resetting and weak zoning of Mn and Ca content.

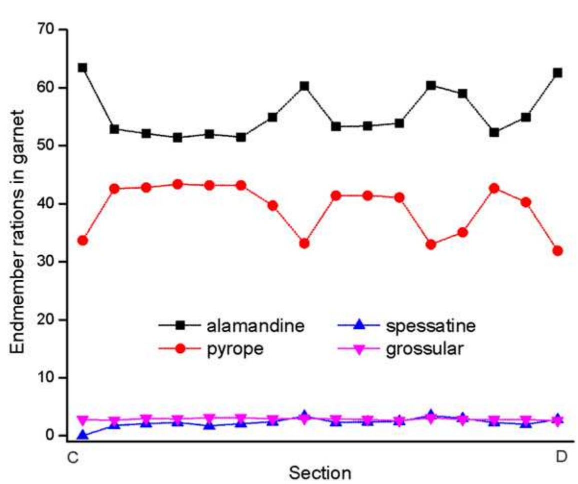

Fig. 8. Profiles showing end-member compositions of garnet in sample Fy0401. The abrupt changes are seen in analytical points adjacent to other Mg–Fe minerals (e.g., biotite, cordierite).

8. Discussion

8.1. Timing of the ultra-high-temperature metamorphism in the Altai orogenic belt

The concordant $^{206}Pb/^{238}U$ age of 277 ± 2 Ma of the zircon overgrowth rims is considered to represent the timing of high-grade metamorphism. Zircon crystals with multifaceted exteriors represent typical products of granulite-facies metamorphism (Corfu et al., 2003; Harley et al., 2007). The concordant ages of the rims may indicate that the diffusion of Pb in the zircon lattice is insignificant at UHT (T > 900 °C) conditions, consistent with the high closure temperature of Pb in zircon (Cherniak and Watson, 2001; Lee et al., 1997). The ages > 300 Ma are mainly detrital and/or inherited from metamorphosed volcano-sedimentary rocks. Specifically, zircon grains with older ages were derived from the Precambrian basement (Yang et al., 2011), whereas zircon grains with Cambrian to Permian ages may represent the magmatic events or regional metamorphic events, such as the metamorphic events during 390 Ma and 470 Ma reported from this region (Long et al., 2007; Yang et al., 2011; Zhang et al., 2012).

The nature of metamorphic zircons from UHT granulites is controlled by their occurrence as well as the chemical composition of the host rock (Harley et al., 2007; Kelsey et al., 2008). The zircon growth in granulite-facies rocks is related to the presence of high-Zr minerals such as Zr released from rutile or during the breakdown of garnet and biotite (Harley et al., 2007). The zircon grain included in cordierite in our study possesses a round shape with a subhedral core showing a

Table 3
Representative compositions of biotite, plagioclase and spinel from the Altay UHT granulite.

Sample no.	Fy0401	Fy0406	Fy0412	FY0401	FY0406	FY0412	FY0401	FY0412
Analysis	5	15	17	406	22	45	535	214-1
Mineral	Biotite	Biotite	Biotite	Plagioclase	Plagioclase	Plagioclase	Spinel	Spinel
SiO_2	36.88	36.86	36.00	60.74	59.90	62.62	0.04	0.00
TiO_2	3.94	3.75	3.65	0.01	0.02	0.00	0.00	0.01
Al_2O_3	18.85	17.76	17.69	25.11	25.68	24.14	60.02	59.18
FeO^T	17.05	17.03	17.34	0.15	0.07	0.05	33.50	30.07
MnO	0.05	–	0.05	0.01	–	–	0.14	0.01
MgO	11.33	11.96	12.24	0.01	0.01	0.01	6.64	7.9
CaO	0.01	0.03	0.04	6.39	7.31	5.59	0.01	0.01
Na_2O	0.17	0.19	0.19	7.90	7.41	8.19	0.02	0.03
K_2O	9.56	10.25	9.53	0.08	0.10	0.22	–	–
Cr_2O_3	–	–	–	–	–	–	–	1.27
ZnO	–	–	–	–	–	–	1.12	2.45
F	0.38	0.40	0.40	–	–	–	–	–
Cl	–	–	–	–	–	–	–	–
Total wt.%	98.22	98.23	97.13	100.38	100.50	100.82	101.48	100.92
No. oxygen	22	22	22	8	8	8	32	32
Si	5.39	5.42	5.36	2.69	2.66	2.75	0.01	–
Al	3.25	3.08	3.10	1.31	1.34	1.25	15.69	15.60
Ti	0.43	0.41	0.41	–	–	–	–	–
Fe^{3+}	–	–	–	–	–	–	–	–
Fe^{2+}	1.88	1.88	1.94	–	–	–	6.21	5.62
Mn	0.01	–	0.01	–	–	–	0.03	–
Mg	2.47	2.62	2.72	–	–	–	2.20	2.63
Ca	–	–	0.01	0.30	0.35	0.26	–	–
Na	0.05	0.05	0.05	0.68	0.64	0.70	0.01	0.01
K	1.78	1.92	1.81	–	0.01	0.01	–	–
Cr	–	–	–	–	–	–	–	0.22
F (right)	0.18	0.19	0.19	–	–	–	–	–
Cl	–	–	–	–	–	–	–	–
Total	15.26	15.40	15.40	4.99	4.99	4.98	24.15	24.09
X(Mg)	0.57	0.58	0.58	–	–	–	0.26	0.32
X(an)	–	–	–	0.31	0.35	0.27	–	–
X(ab)	–	–	–	0.69	0.64	0.72	–	–
X(or)	–	–	–	0.00	0.01	0.01	–	–

different optical characteristic (see Fig. 3e and f). Cordierite is a reaction product of the breakdown of garnet during the near-isothermal decompression (ITD) stage. A near-ITD followed by an isobaric cooling (IBC) retrograde P–T path was also accompanied by progressive melting. Therefore, the zircon grains in this study may have crystallized during the decompression and cooling stage of melt according to the pseudosection modeling in the NCKFMASHTZr system (Kelsey and Powell, 2011). The wide age span from 269 ± 2 Ma to 286 ± 4 Ma may be consistent with the continuous growth of zircon grains during the decompression and cooling stage. Therefore, we interpret the metamorphic ages of 269–286 Ma with a weighted mean $^{206}Pb/^{238}U$ age of 277 ± 2 Ma to represent the timing of the decompression and cooling stage rather than the peak stage. These results are further supported by deformed and undeformed granitic plutons in the Fuyun area, which have TIMS zircon U–Pb ages of 281 ± 5 Ma and 275 ± 2 Ma, respectively. The ages are interpreted to mark the time of compression to extension (decompression) in this region (Tong et al., 2006).

8.2. An anti-clockwise P–T–t path of the Altai UHT granulite

The UHT granulite facies conditions in the Altai UHT belt are confirmed by the assemblage of high-Al orthopyroxene + sillimanite ± quartz in this study. Considering that spinel + quartz is stable at a pressure lower than that of orthopyroxene + sillimanite, the mineral inclusion of spinel + quartz + sillimanite (and/or cordierite) in the core of garnet is regarded to have developed in the prograde stage (M0) although no robust textures exist to precisely constraint the metamorphic sequence of the two mineral assemblages. The mineral assemblages developed in the granulite and P–T conditions constrained from pseudosections therefore define an anti-clockwise P–T path (Fig. 10). The decompression reaction contributed to the formation of cordierite corona at the expense of garnet, which might have been accompanied by the rim growth of Type 1 zircon grains. The SHRIMP zircon U–Pb age of the sillimanite schist in the andalusite–sillimanite zone reveals that the andalusite-type metamorphism (635–670 °C and 5.8–6.8 kbar) occurred at 299.2 ± 3.4 Ma (Wang et al., 2013), and the low-pressure pelitic granulite-facies metamorphism (780–800 °C and 5.0–6.0 kbar) in the sillimanite zone at 292.8 ± 2.8 Ma (W. Wang et al., 2009), indicating that a continuous heat flux occurred in the region during this period. We therefore infer that the 299.2 ± 3.4 Ma age may represent the onset of the thermal event, whereas the 292.8 ± 2.8 Ma age corresponds to the peak or pre-peak metamorphic event of the Altai UHT granulite. The zircon U–Pb ages of 286 ± 4 to 269 ± 2 Ma obtained in this study may represent the retrograde stage. The anti-clockwise UHT metamorphic P–T–t path obtained in this study and the P–T paths from other metamorphic zones in the Altai orogenic belt (after Wei et al., 2007) are summarized in Fig. 10.

Granulite facies metamorphic rocks formed by the orogenic process are commonly characterized by clockwise P–T paths (England and Richardson, 1977; Thompson and England, 1984). However, recent studies show that several HT–UHT granulites possess anti-clockwise P–T paths, particularly those which witnessed subduction and accretion processes, such as the Qinling–Tongbai orogen in Central China (Xiang et al., 2012), the Khondalite belt of the North China Craton (Santosh et al., 2009), the Palghat–Cauvery Shear Zone (Gondwana suture) in southern India (Santosh and Sajeev, 2006), the eastern Ghats Belt in East India (Korhonen et al., 2011), and the Sør Rondane Mountains in East Antarctica (Baba et al., 2013; Nakano et al., 2013). The studies in these belts also indicate that the retrograde metamorphism characterized by isobaric cooling (IBC) or isothermal decompression (ITD) trajectories may have occurred along both a clockwise and anti-clockwise P–T loop (Santosh and Sajeev, 2006).

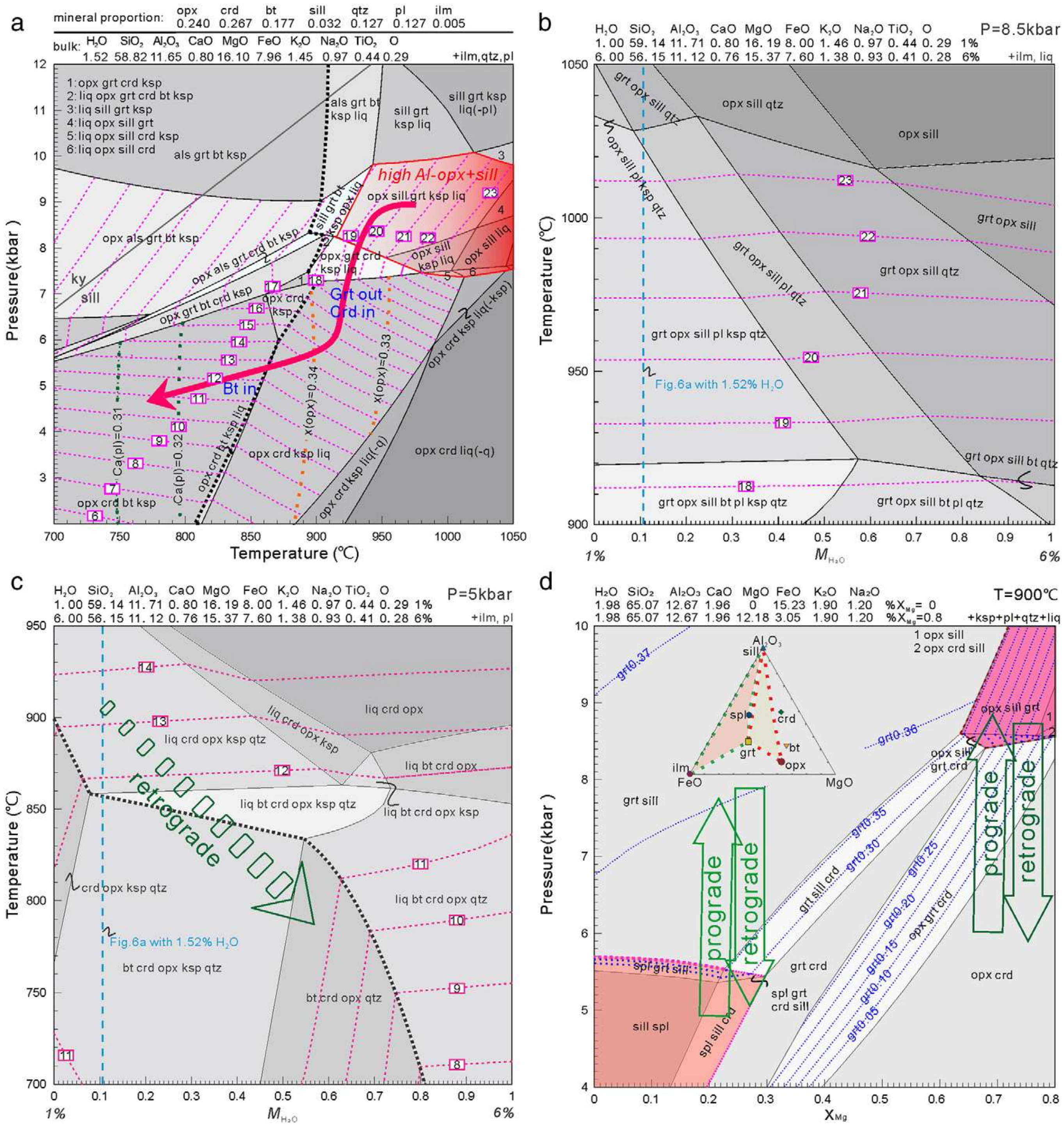

Fig. 9. (a) Pseudosection constructed in Na_2O–CaO–K_2O–FeO–MgO–Al_2O_3–SiO_2–H_2O–TiO_2–Fe_2O_3 for the Altai UHT granulite from the effective bulk composition (Fig. 3h); (b) and c) T–M_{H2O} pseudosection modeling with the same composition at 8.5 kbar and 5.0 kbar, respectively; d) T–X_{Mg} pseudosection showing different mineral assemblages due to heterogeneous bulk compositions with spinel in the low X_{Mg} side and orthopyroxene in the high X_{Mg} side. Note: Pink dashed lines show the y(opx) isopleths (×100) which are perpendicular/near perpendicular to the temperature axis (≥12). Blue isopleths in Fig. 9d show the mole proportion of garnet, suggesting garnet growth with pressure increases and breakdown with pressure decreases. Triangle in (d) shows the projection of mineral composition.

8.3. Implications for the early Permian UHT event in the Altai orogenic belt

The UHT metamorphism in exhumed hinterlands of orogens has been taken to indicate that temperatures >900 °C could be achieved and sustained during crustal metamorphism (Brown, 2007). Because of the gradual "cooling" of the earth or the long time taken for crustal rocks to ascend from the deep crust to the surface, regional UHT metamorphism is relatively rare in the Phanerozoic terranes (especially those younger than 500 Ma). Only a few examples have been reported so far, such as the Seram UHT rocks in East Indonesia (16 Ma, Pownall et al., 2014), the Gruf Unit in the central Alps (~33 Ma, Liati and Gebauer, 2003; ~272 Ma, Galli et al., 2011) and Qinling–Tongbai orogen (~432 Ma, Xiang et al., 2012). The Permian UHT granulite in the Altai orogenic belt thus provides another good example of extreme

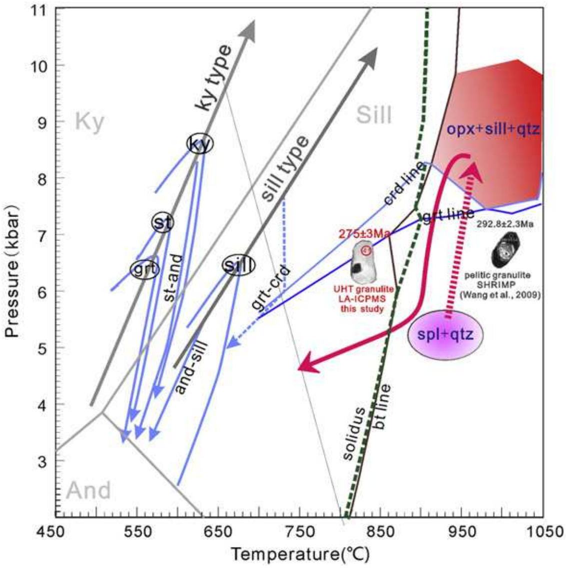

Fig. 10. A P–T–t diagram showing the anticlockwise P–T path of the Altai UHT granulite. Data source: P–T paths in blue arrows are from Wei et al. (2007).

thermal metamorphism of the crust in the late Paleozoic plate tectonic regime.

The Altai orogenic belt experienced a prolonged tectonic history associated with the northward subduction of the Kazakhstan–Junggar plate beneath the Siberian plate during the Paleozoic. The timing of the termination of the accretion–collision process is debated with models proposing early Carboniferous (Wang et al., 2006) or Triassic (Xiao et al., 2010) ages. However, post-orogenic granites with ages of 320 to 290 Ma are reported in the Altai orogenic belt (Wang et al., 2006; Yuan et al., 2007). The sillimanite schist in the andalusite–sillimanite zone was dated as 299.2 ± 3.4 Ma (Wang et al., 2013) and the pelitic granulite yielded an age of 292.8 ± 2.8 Ma (W. Wang et al., 2009), indicating that the heat flux may have developed at intermediate to low pressure conditions. During 290 to 280 Ma, the clockwise rotation of the Siberian plate and the northward movement of the Kazakhstan–Junggar plate resulted in the sinistral strike-slip (Buslov et al., 2004; Laurent-Charvet et al., 2003). The granitic plutons (286–267 Ma), ultramafic–mafic intrusions (287–273 Ma), and bimodal mafic and silicic dykes (276–252 Ma) formed in the belt (Zhang et al., 2012) under an extensional setting. The Tarim mantle plume may have contributed to the magmatism in the northern Xinjiang region during the early Permian (Qin et al., 2011; Zhang et al., 2012).

Based on the anti-clockwise P–T–t trajectory (Fig. 10) and the timing of tectonic events of the Altai orogenic belt, we propose the following tectonic scenario during the late Paleozoic evolution of the region. Successive northward subduction of the Kazakhstan–Junggar plate and the slab break-off which caused asthenospheric upwelling and heat flux at 320–290 Ma may contribute to high-grade metamorphism generating the sillimanite schist and pelitic granulite (W. Wang et al., 2009, 2013) and the UHT granulite at deep levels (ca. 27–34 km), with the emplacement of coeval mafic–ultramafic intrusions and felsic plutons. The rotation of the Siberian plate and the Kazakhstan–Junggar plate caused local compression, leading to the increase of pressure from the stability field of spinel + quartz to orthopyroxene + sillimanite so that sufficient shear heat was generated to form gneissic granite. Subsequent exhumation led to decompression from ~8 kbar to ~5 kbar. The zircon grains in the cordierite corona may have crystallized during this stage and the low-density carbonic fluid inclusions occurring in these rocks are probably a result of density reversal due to the modification of the inclusion cavity volume during rapid decompression (Yang and Li, 2013). We conclude that the formation of the Altai UHT granulite is related to the sinistral strike-slip motion along the Irtish tectonic belt after the subduction and slab detachment processes.

9. Conclusions

The diagnostic mineral assemblages of orthopyroxene + sillimanite + quartz and low-Zn spinel + quartz characterize the Altai UHT granulite. Cordierite corona surrounding high-Al orthopyroxene resulted from post-peak decompression. Replacement of high-Al orthopyroxene by the symplectite of low-Al orthopyroxene and cordierite is a result of the decompression process. The low-Al orthopyroxene and garnet were replaced by biotite in the final cooling stage. The Altai UHT granulite was exhumed along an anti-clockwise P–T trajectory with the pre-peak assemblage of spinel + quartz in garnet formed at >940 °C and 7.8–10 kbar, followed by near-isothermal decompression at 890–940 °C and 5–6 kbar and a final-stage cooling at 750–800 °C and 4–5 kbar. The zircon U–Pb age of 277 ± 2 Ma from the UHT granulite is interpreted to mark the timing of decompression and cooling processes. The Altai UHT granulite may have formed in an extensional setting during the sinistral strike-slip motion along the Irtish belt after the subduction and slab detachment processes.

Acknowledgements

We thank the Editor and referees for their valuable comments which improved this paper. The authors express sincere thanks to J.Z. Geng and H.K. Li of the Tianjing Institute of Geology and Mineral Resources for their assistance in LA–MC–ICP-MS zircon U–Pb dating, H.H. Wang of Zhejiang University for his assistance in field and indoor work, J.H. Zhu of the Key Laboratory of the Second Institute of Oceanography of the State Oceanic Administration in Hangzhou, China for assistance in EPMA analysis, and B. Song (Beijing SHRIMP Center of China, Institute of Geology, Chinese Academy of Geological Sciences) for experimental guidance and recalculation of age data. This study was financially supported by the National Basic Research Program of China (973 Program: 2011CB808902), the National Natural Science Foundation of China (Grant Nos. 40972045 and 41072048), and the Research Fund for the Doctoral Program of Higher Education of China (Grant No. 20110101110001). This study also contributes to the Talent Award to M. Santosh under the 1000 Talents Plan of the Chinese Government.

Appendix A. Supplementary data

Supplementary data to this article can be found online at http://dx.doi.org/10.1016/j.lithos.2014.05.022.

References

Alvarez-Valero, A.M., Waters, D.J., 2010. Partially melted crustal xenoliths as a window into sub-volcanic processes: evidence from the Neogene magmatic province of the Betic Cordillera, SE Spain. Journal of Petrology 51, 973–991.

Baba, S., Osanai, Y., Nakano, N., Owada, M., Hokada, T., Horie, K., Adachi, T., Toyoshima, T., 2013. Counterclockwise P–T path and isobaric cooling of metapelites from Brattnipene, Sør Rondane Mountains, East Antarctica: implications for a tectonothermal event at the proto-Gondwana margin. Precambrian Research 234, 210–228.

Brown, M., 2006. Duality of thermal regimes is the distinctive characteristic of plate tectonics since the Neoarchean. Geology 34, 961–964.

Brown, M., 2007. Metamorphic conditions in orogenic belts: a record of secular change. International Geology Review 49, 193–234.

Brown, M., 2014. The contribution of metamorphic petrology to understanding lithosphere evolution and geodynamics. Geoscience Frontiers. http://dx.doi.org/10.1016/j.gsf.2014.02.005.

Buslov, M.M., Watanabe, T., Fujiwara, Y., Iwata, K., Smirnova, L.V., Safonova, I.Y., Semakov, N.N., Kiryanova, A.P., 2004. Late Paleozoic faults of the Altai region, Central Asia: tectonic pattern and model of formation. Journal of Asian Earth Sciences 23, 655–671.

Chen, B., Jahn, B.M., 2002. Geochemical and isotopic studies of the sedimentary and granitic rocks of the Altai orogen of northwest China and their tectonic implications. Geological Magazine 139, 1–13.

Chen, H.L., Yang, S.F., Li, Z.L., Yu, X., Xiao, W.J., Yuan, C., Lin, X.B., Li, J.L., 2006. Zircon SHRIMP U–Pb chronology of Fuyun basic granulite and its tectonic significance in Altaid orogenic belt. Acta Petrologica Sinica 22, 1351–1358 (in Chinese with English abstract).

Cherniak, D., Watson, E., 2001. Pb diffusion in zircon. Chemical Geology 172, 5–24.

Clark, C., Fitzsimons, I.C.W., Healy, D., Harley, S.L., 2011. How does the continental crust get really hot? Elements 7, 235–240.

Clarke, G., Daczko, N., Nockolds, C., 2001. A method for applying matrix corrections to X-ray intensity maps using the Bence–Albee algorithm and Matlab. Journal of Metamorphic Geology 19, 635–644.

Corfu, F., Hanchar, J.M., Hoskin, P.W., Kinny, P., 2003. Atlas of zircon textures. Reviews in Mineralogy and Geochemistry 53, 469–500.

Dharma Rao, C.V., Santosh, M., Chmielowski, R.M., 2012. Sapphirine granulites from Panasapattu, Eastern Ghats belt, India: ultrahigh-temperature metamorphism in a Proterozoic convergent plate margin. Geoscience Frontiers 3, 9–31.

England, P.C., Richardson, S., 1977. The influence of erosion upon the mineral fades of rocks from different metamorphic environments. Journal of the Geological Society 134, 201–213.

Galli, A., Le Bayon, B., Schmidt, M.W., Burg, J.P., Caddick, M.J., Reusser, E., 2011. Granulites and charnockites of the Gruf Complex: evidence for Permian ultra-high temperature metamorphism in the Central Alps. Lithos 124, 17–45.

Guiraud, M., Powell, R., Rebay, G., 2001. H_2O in metamorphism and unexpected behaviour in the preservation of metamorphic mineral assemblages. Journal of Metamorphic Geology 19, 445–454.

Harley, S.L., 2004. Extending our understanding of ultrahigh temperature crustal metamorphism. Journal of Mineralogical and Petrological Sciences 99, 140–158.

Harley, S.L., 2008. Refining the P–T records of UHT crustal metamorphism. Journal of Metamorphic Geology 26, 125–154.

Harley, S.L., Kelly, N.M., Moller, A., 2007. Zircon behaviour and the thermal histories of mountain chains. Elements 3, 25–30.

He, G.Q., Han, B.F., Yue, Y.J., 1990. The tectonic evolution of Chinese Altai. Xinjiang Geology 2, 9–20 (in Chinese).

Holland, T.J.B., Powell, R., 1998. An internally consistent thermodynamic data set for phases of petrological interest. Journal of Metamorphic Geology 16, 309–343.

Holland, T., Powell, R., 2003. Activity–composition relations for phases in petrological calculations: an asymmetric multicomponent formulation. Contributions to Mineralogy and Petrology 145, 492–501.

Holness, M.B., Cesare, B., Sawyer, E.W., 2011. Melted rocks under the microscope: microstructures and their interpretation. Elements 7, 247–252.

Hu, A., Zhang, G., Zhang, Q., Li, T., Zhang, J., 2002. A review on ages of Precambrian metamorphic rocks from Altai orogen in Xinjiang, NW China. Scientia Geologica Sinica 2, 129–142 (in Chinese with English abstract).

Iizuka, T., Hirata, T., 2005. Improvements of precision and accuracy in in situ Hf isotope microanalysis of zircon using the laser ablation–MC–ICPMS technique. Chemical Geology 220, 121–137.

Jiang, Y., Sun, M., Zhao, G., Yuan, C., Xiao, W., Xia, X., Long, X., Wu, F., 2011. The ~390 Ma high-T metamorphic event in the Chinese Altai: a consequence of ridge-subduction? American Journal of Science 310, 1421–1452.

Kelsey, D.E., 2008. On ultrahigh-temperature crustal metamorphism. Gondwana Research 13, 1–29.

Kelsey, D.E., Powell, R., 2011. Progress in linking accessory mineral growth and breakdown to major mineral evolution in metamorphic rocks: a thermodynamic approach in the $Na_2O–CaO–K_2O–FeO–MgO–Al_2O_3–SiO_2–H_2O–TiO_2–ZrO_2$ system. Journal of Metamorphic Geology 29, 151–166.

Kelsey, D.E., Clark, C., Hand, M., 2008. Thermobarometric modelling of zircon and monazite growth in melt-bearing systems: examples using model metapelitic and metapsammitic granulites. Journal of Metamorphic Geology 26, 199–212.

Korhonen, F.J., Saw, A.K., Clark, C., Brown, M., Bhattacharya, S., 2011. New constraints on UHT metamorphism in the Eastern Ghats Province through the application of phase equilibria modelling and in situ geochronology. Gondwana Research 20, 764–781.

Laurent-Charvet, S., Charvet, J., Monie, P., Shu, L.S., 2003. Late Paleozoic strike-slip shear zones in eastern central Asia (NW China): new structural and geochronological data. Tectonics 22.

Lee, J.K., Williams, I.S., Ellis, D.J., 1997. Pb, U and Th diffusion in natural zircon. Nature 390, 159–162.

Li, Z.L., Li, Y.Q., Chen, H.L., Santosh, M., Xiao, W.J., Wang, H.H., 2010a. SHRIMP U–Pb zircon chronology of ultrahigh-temperature spinel–orthopyroxene–garnet granulite from South Altay orogenic belt, northwestern China. Island Arc 19, 506–516.

Li, Z.L., Wang, H.H., Chen, H.L., Xiao, W.J., Yang, S.F., Hu, Y.Z., 2010b. Composition of spinels, spinel–quartz association and mineral reactions from ultrahigh-temperature granulites: an example from spinel–orthopyroxene–garnet granulite of the South Allay orogenic belt. Earth Science Frontiers 17, 74–85 (in Chinese with English abstract).

Li, Z.-l., Chen, H.-l., Santosh, M., Yang, S.-f., 2004. Discovery of Li, Z.L., Chen, H.L., Yang, S.F., Dong, C.W., Xiao, W.J., 2004. Petrology, geochemistry and geodynamics of basic granulite from the Altay area, North Xinjiang, China. Journal of Zhejiang University Science 5, 979–984.

Liati, A., Gebauer, D., 2003. Geochronological constraints for the time of metamorphism in the Gruf Complex (Central Alps) and implications for the Adula-Cima Lunga nappe system. Schweizerische Mineralogische und Petrographische Mitteilungen 83, 159–172.

Long, X.P., Sun, M., Yuan, C., Xiao, W.J., Lin, S.F., Wu, F., Xia, X.P., Cai, K.D., 2007. Detrital zircon age and Hf isotopic studies for metasedimentary rocks from the Chinese Altai: implications for the early Paleozoic tectonic evolution of the central Asian orogenic belt. Tectonics 26.

Long, X.P., Yuan, C., Sun, M., Xiao, W.J., Zhao, G.C., Wang, Y.J., Cai, K.D., Xia, X.P., Xie, L.W., 2010. Detrital zircon ages and Hf isotopes of the early Paleozoic flysch sequence in the Chinese Altai, NW China: new constrains on depositional age, provenance and tectonic evolution. Tectonophysics 480, 213–231.

Ludwig, K., 2009. Isoplot 4.1. A geochronological toolkit for Microsoft Excel. Berkeley Geochronology Center Special, Publication, 4, p. 76.

Nabelek, P.I., Whittington, A.G., Hofmeister, A.M., 2010. Strain heating as a mechanism for partial melting and ultrahigh temperature metamorphism in convergent orogens: implications of temperature-dependent thermal diffusivity and rheology. Journal of Geophysical Research - Solid Earth 115.

Nakano, N., Osanai, Y., Kamei, A., Satish-Kumar, M., Adachi, T., Hokada, T., Baba, S., Toyoshima, T., 2013. Multiple thermal events recorded in metamorphosed carbonate and associated rocks from the southern Austkampane region in the Sør Rondane Mountains, East Antarctica: a protracted Neoproterozoic history at the Gondwana suture zone. Precambrian Research 234, 161–182.

Nichols, G.T., Berry, R.F., Green, D.H., 1992. Internally consistent gahnitic spinel–cordierite–garnet equilibria in the FMASHZn system — geothermobarometry and applications. Contributions to Mineralogy and Petrology 111, 362–377.

Pattison, D.R.M., Chacko, T., Farquhar, J., McFarlane, C.R.M., 2003. Temperatures of granulite-facies metamorphism: constraints from experimental phase equilibria and thermobarometry corrected for retrograde exchange. Journal of Petrology 44, 867–900.

Powell, R., Holland, T.J.B., 1988. An internally consistent dataset with uncertainties and correlations: 3. Applications to geobarometry, worked examples and a computer program. Journal of Metamorphic Geology 6, 173–204.

Pownall, J.M., Hall, R., Armstrong, R.A., Forster, M.A., 2014. Earth's youngest known ultrahigh-temperature granulites discovered on Seram, eastern Indonesia. Geology G35230, 35231.

Qin, K.Z., Su, B.X., Sakyi, P.A., Tang, D.M., Li, X.H., Sun, H., Xiao, Q.H., Liu, P.P., 2011. SIMS zircon U-Pb geochronology and Sr-Nd isotopes of Ni-Cu-Bearing Mafic-Ultramafic Intrusions in Eastern Tianshan and Beishan in correlation with flood basalts in Tarim Basin (NW China): Constraints on a ca. 280 Ma mantle plume. American Journal of Science 311, 237–260.

Santosh, M., Kusky, T., 2010. Origin of paired high pressure-ultrahigh-temperature orogens: a ridge subduction and slab window model. Terra Nova 22, 35–42.

Santosh, M., Omori, S., 2008. CO_2 windows from mantle to atmosphere: models on ultrahigh-temperature metamorphism and speculations on the link with melting of snowball Earth. Gondwana Research 14, 82–96.

Santosh, M., Sajeev, K., 2006. Anticlockwise evolution of ultrahigh-temperature granulites within continental collision zone in southern India. Lithos 92, 447–464.

Santosh, M., Sajeev, K., Li, J.H., Liu, S.J., Itaya, T., 2009. Counterclockwise exhumation of a hot orogen: the Paleoproterozoic ultrahigh-temperature granulites in the North China Craton. Lithos 110, 140–152.

Santosh, M., Liu, S.J., Tsunogae, T., Li, J.H., 2012. Paleoproterozoic ultrahigh-temperature granulites in the North China Craton: implications for tectonic models on extreme crustal metamorphism. Precambrian Research 222–223, 77–106.

Shimizu, H., Tsunogae, T., Santosh, M., 2013. Petrology and phase equilibrium modeling of sapphirine + quartz assemblage from the Napier Complex, East Antarctica: diagnostic evidence for Neoarchean ultrahigh-temperature metamorphism. Geoscience Frontiers 6, 655–666.

Spear, F., 1993. Metamorphic phase equilibria and pressure–temperature–time paths. Mineralogical Society of America Monograph, Book Crafters.

Thompson, A.B., England, P.C., 1984. Pressure–temperature–time paths of regional metamorphism II. Their inference and interpretation using mineral assemblages in metamorphic rocks. Journal of Petrology 25, 929–955.

Tong, Y., Hong, D., Wang, T., Wang, S., Han, B., 2006. TIMS U–Pb zircon ages of Fuyun post-orogenic linear granite plutons on the southern margin of Altay orogenic belt and their implications. Acta Petrologica et Mineralogica 25, 85–89 (in Chinese with English abstract).

Tong, Y., Wang, T., Siebel, W., Hong, D.-W., Sun, M., 2012. Recognition of early Carboniferous alkaline granite in the southern Altai orogen: post-orogenic processes constrained by U–Pb zircon ages, Nd isotopes, and geochemical data. International Journal of Earth Sciences 101, 937–950.

Tsunogae, T., Liu, S.J., Santosh, M., Shimizu, H., Li, J.H., 2011. Ultrahigh-temperature metamorphism in Daqingshan, Inner Mongolia Suture Zone, North China. Gondwana Research 20, 36–47.

Wang, T., Hong, D.W., Jahn, B.M., Tong, Y., Wang, Y.B., Han, B.F., Wang, X.X., 2006. Timing, petrogenesis, and setting of Paleozoic synorogenic intrusions from the Altai Mountains, northwest China: implications for the tectonic evolution of an accretionary orogen. Journal of Geology 114, 735–751.

Wang, W., Wei, C., Wang, T., Lou, Y., Chu, H., 2009a. Confirmation of pelitic granulite in the Altai orogen and its geological significance. Chinese Science Bulletin 54, 2543–2548 (in Chinese with English abstract).

Wang, T., Jahn, B.M., Kovach, V.P., Tong, Y., Hong, D.W., Han, B.F., 2009b. Nd–Sr isotopic mapping of the Chinese Altai and implications for continental growth in the Central Asian Orogenic Belt. Lithos 110, 359–372.

Wang, Y., Yuan, C., Long, X., Sun, M., Xiao, W., Zhao, G., Cai, K., Jiang, Y., 2011. Geochemistry, zircon U–Pb ages and Hf isotopes of the Paleozoic volcanic rocks in the northwestern Chinese Altai: petrogenesis and tectonic implications. Journal of Asian Earth Sciences 42, 969–985.

Wang, W., Wei, C., Zhang, Y., Chu, H., Zhao, Y., Liu, X., 2013. Age and origin of sillimanite schist from the Chinese Altai metamorphic belt: implications for late Paleozoic tectonic evolution of the Central Asian Orogenic Belt. International Geology Review 1–13.

Wei, C., Clarke, G., Tian, W., Qiu, L., 2007. Transition of metamorphic series from the kyanite- to andalusite-types in the Altai orogen, Xinjiang, China: evidence from petrography and calculated KMnFMASH and KFMASH phase relations. Lithos 96, 353–374.

White, R.W., Powell, R., Holland, T.J.B., Worley, B.A., 2000. The effect of TiO_2 and Fe_2O_3 on metapelitic assemblages at greenschist and amphibolite facies conditions: mineral equilibria calculations in the system K_2O–FeO–MgO–Al_2O_3–SiO_2–H_2O–TiO_2–Fe_2O_3. Journal of Metamorphic Geology 18, 497–511.

White, R.W., Powell, R., Clarke, G.L., 2002. The interpretation of reaction textures in Fe-rich metapelitic granulites of the Musgrave Block, central Australia: constraints from mineral equilibria calculations in the system K_2O–FeO–MgO–Al_2O_3–SiO_2–H_2O–TiO_2–Fe_2O_3. Journal of Metamorphic Geology 20, 41–55.

White, R.W., Powell, R., Holland, T.J.B., 2007. Progress relating to calculation of partial melting equilibria for metapelites. Journal of Metamorphic Geology 25, 511–527.

Windley, B.F., Kröner, A., Guo, J., Qu, G., Li, Y., Zhang, C., 2002. Neoproterozoic to Paleozoic geology of the Altai orogen, NW China: new zircon age data and tectonic evolution. The Journal of Geology 110, 719–737.

Windley, B.F., Alexeiev, D., Xiao, W.J., Kroner, A., Badarch, G., 2007. Tectonic models for accretion of the central Asian orogenic belt. Journal of the Geological Society 164, 31–47.

Xiang, H., Zhang, L., Zhong, Z.-Q., Santosh, M., Zhou, H.-W., Zhang, H.-F., Zheng, J.-P., Zheng, S., 2012. Ultrahigh-temperature metamorphism and anticlockwise P–T–t path of Paleozoic granulites from north Qinling–Tongbai orogen, Central China. Gondwana Research 21, 559–576.

Xiao, W., Santosh, M., 2014. The western Central Asian Orogenic Belt: a window to accretionary orogenesis and continental growth. Gondwana Research 25, 1429–1444.

Xiao, W.J., Windley, B.F., Huang, B.C., Han, C.M., Yuan, C., Chen, H.L., Sun, M., Sun, S., Li, J.L., 2009. End-Permian to mid-Triassic termination of the accretionary processes of the southern Altaids: implications for the geodynamic evolution, Phanerozoic continental growth, and metallogeny of Central Asia. International Journal of Earth Sciences 98, 1189–1217.

Xiao, W.J., Huang, B.C., Han, C.M., Sun, S., Li, J.L., 2010. A review of the western part of the Altaids: a key to understanding the architecture of accretionary orogens. Gondwana Research 18, 253–273.

Yang, X.Q., Li, Z.L., 2013. Fluid characteristics of Late Paleozoic ultrahigh-temperature granulite from the Altay orogenic belt, northwestern China and its significance. Acta Petrologica Sinica 29, 3446–3456 (in Chinese with English abstract).

Yang, T.N., Li, J.Y., Zhang, J., Hou, K.J., 2011. The Altai-Mongolia terrane in the Central Asian Orogenic Belt (CAOB): a peri-Gondwana one? Evidence from zircon U–Pb, Hf isotopes and REE abundance. Precambrian Research 187, 79–98.

Yuan, C., Sun, M., Xiao, W., Li, X., Chen, H., Lin, S., Xia, X., Long, X., 2007. Accretionary orogenesis of the Chinese Altai: insights from Paleozoic granitoids. Chemical Geology 242, 22–39.

Zhang, C.L., Santosh, M., Zou, H.B., Xu, Y.G., Zhou, G., Dong, Y.G., Ding, R.F., Wang, H.Y., 2012. Revisiting the "Irtish tectonic belt": implications for the Paleozoic tectonic evolution of the Altai orogen. Journal of Asian Earth Sciences 52, 117–133.

Zheng, C.Q., Kato, T., Enami, M., Xu, X.C., 2007. CHIME monazite ages of metasediments from the Altai orogen in northwestern China: Devonian and Permian ages of metamorphism and their significance. Island Arc 16, 598–604.

Zhuang, Y.X., 1994. Tectonothermal Evolution in Space and Time and Orogenic Process of Altaide, China. Jilin Scientific and Technical Press, Changchun, China, (in Chinese with English abstract).